archaeometry

Archaeometry ••, •• (2016) ••–•• doi: 10.1111/arcm.12245

FULL-VECTOR ARCHAEOMAGNETIC DATING OF A MEDIEVAL LIMEKILN AT PINILLA DEL VALLE SITE (MADRID, SPAIN)*

Á. CARRANCHO†

Área de Prehistoria, Departamento de Historia, Geografía y Comunicación, Universidad de Burgos, Edificio I+D+I, Plaza Misael Bañuelos s/n 09001, Burgos, Spain

A. GOGUITCHAICHVILI and J. MORALES

Servicio Arqueomagnético Nacional y Laboratorio Interinstitucional de Magnetismo Natural (LIMNA), Instituto de Geofísica, Unidad Michoacán, Campus Morelia, Universidad Nacional Autónoma de México, México

J. A. ESPINOSA-SOTO

Centro Internacional Estudios Multimedia de Madrid (CIEMAD), C/ Químicas 2, 1ª planta, oficina 1.3; 28925 Alcorcón, Madrid, Spain

J. J. VILLALAÍN

Departamento de Física, Universidad de Burgos, Escuela Politécnica Superior, Avda. Cantabria S/N 09006, Burgos, Spain

J. L. ARSUAGA

Centro de Evolución y Comportamiento Humanos (UCM-ISCIII), Instituto de Salud Carlos III, C/ Monforte de Lemos 5, Pabellón 14, 2802, Madrid, Spain and Departamento de Palaeontología, Facultad de Ciencias Geológicas, Universidad Complutense de Madrid, 28040, Madrid, Spain

E. BAQUEDANO

Museo Arqueológico Regional de la Comunidad de Madrid, Plaza de las Bernardas, s/n, 28801—Alcalá de Henares, Madrid, Spain and IDEA (Instituto de Evolución en África), Museo de los Orígenes, Plaza de San Andrés 2, 28005, Madrid, Spain

and A. PÉREZ-GONZÁLEZ

CENIEH (Centro Nacional de Investigación sobre la Evolución Humana), Paseo Sierra de Atapuerca s/n, 9002 Burgos, Spain

Archaeomagnetic dating based on the full geomagnetic field vector was carried out on a limekiln excavated at Pinilla del Valle archaeological site (Madrid, Spain). The limekiln tradition in this area is largely documented by historical sources for recent centuries but the date of the studied kiln's last use was unknown. The combination of mean archaeomagnetic directional and absolute archaeointensity results shows that the kiln was last used between AD 1296 and 1413, in good agreement with two independent radiocarbon dates. This study provides the first archaeomagnetic evidence that the local limekiln tradition dates back to at least late medieval times. Furthermore, the inclusion of these data in the Iberian secular variation curve and geomagnetic field models will help to improve the archaeomagnetic dating technique.

*Received 24 September 2014; accepted 2 February 2016
†Corresponding author: email acarrancho@ubu.es

KEYWORDS: ARCHAEOMAGNETISM, ARCHAEOINTENSITY, SECULAR VARIATION, THERMOREMANENCE, ROCK AND MINERAL MAGNETISM, MIDDLE AGES, IBERIAN PENINSULA

INTRODUCTION

In recent years, there has been considerable progress in the application of archaeomagnetism as a dating method in archaeology. The construction of regional secular variation curves (SVC) of the Earth's magnetic field in various regions, such as the American Southwest (e.g., Hagstrum and Blinman 2010; Lengyel 2010), the Near East (e.g., Stillinger *et al.* 2015) and mainly in Europe (e.g., Gallet *et al*. 2002; Schnepp and Lanos 2005; Gómez-Paccard *et al*. 2006a; Tema *et al.* 2006; Zananiri *et al*. 2007; Kovacheva *et al*. 2009), as well as the computation of regional geomagnetic models (Pavón-Carrasco *et al*. 2009) make archaeomagnetic dating possible on archaeological sites for the past two or three millennia (e.g., Prevosti *et al*. 2013; Tema *et al*. 2013). Likewise, older time periods are progressively being encompassed (e.g., Tema and Kondopoulou 2011; Carrancho *et al*. 2013; Kapper *et al*. 2014).

Any archaeological material containing ferromagnetic minerals (*s.l.*) that have undergone high-temperature heating ($>$ 500–600 °C) can, under certain conditions, record the direction and/or intensity of the Earth's magnetic field at the time of its last heating and subsequent cooling through the acquisition of a thermoremanent magnetization (TRM). The mechanism of TRM acquisition relies on the capacity of some ferromagnetic minerals (mainly iron oxides and hydroxides) to retain a remanent magnetization. In directional studies, it is crucial that the material remains undisturbed from its original position during the last heating (still *in situ*). Otherwise, the originally recorded direction of the Earth's magnetic field would lack a geographical orientation, as happens with pottery fragments. If the material does not undergo subsequent reheatings or physicochemical alterations, the TRM acquired, parallel and proportional to the ambient magnetic field, may remain stable over time. Standard archaeomagnetic dating procedures are based on the comparison of the direction and/or intensity of the Earth's magnetic field recorded in the material with the SVC available for the time period and region concerned. This is necessary because the SV is a phenomenon that is reproducible for regions of no more than 600–900 km of radius (Lanos 2004). Therefore, *in situ* burnt materials that fulfill those requirements, such as kilns, furnaces or bricks, are among the most suitable for dating by archaeomagnetism.

In the Iberian Peninsula, Gómez-Paccard *et al*. (2006a) has published a SVC for the past two millennia and, later, Pavón-Carrasco *et al*. (2009) has produced a European geomagnetic field model (SCHA.DIF.3 K) enabling the use of archaeomagnetism as a dating tool in this area. Here, we use archaeomagnetism to constrain the age of the last firing of a limekiln at Pinilla del Valle site (Madrid, central Spain). Although the archaeomagnetic literature about kilns is large, the studies specifically carried out on archaeological limekilns are relatively scarce. Hus and Geeraerts (1998) studied and dated two quicklime kilns using the British and French SVCs as reference curves in their trial to construct a PSV for Belgium. Borradaile *et al*. (2001), unable to perform thermal demagnetization due to the friable nature of magnetite-bearing claystone samples from a limekiln in UK, applied low-temperature demagnetization (LTD) followed by AF demagnetization to successfully isolate the characteristic remanent magnetization (ChRM) direction, inferring a late medieval last use of the kiln. Tema and Lanza (2008) used the Italian and French SVCs to date a limekiln in northern Italy, obtaining reproducible results and estimating that the last firing could have occurred as late as the end of the sixth century AD. Donadini *et al*. (2010) studied and dated several Roman limekilns in Bulgaria and, more

recently, Casas *et al.* (2014) combined archaeomagnetic (directional) and thermoluminiscence methods to date two limekilns in north-eastern Spain to the mid-19th century AD. Despite that, much remains to be studied about these structures to evaluate their potential as geomagnetic field recorders and their suitability for archaeomagnetic dating. Our study aims to show how reliably this limekiln has recorded the direction and intensity of the Earth's magnetic field and to determine the age of its last use. The archaeomagnetic dating interval obtained is compared to two available radiocarbon dates. To our knowledge, as yet there is no study carried out on limekilns combining direction, intensity and ^{14}C dating. Finally, the archaeological and geomagnetic implications of the results are discussed.

MATERIAL AND METHODS

Site description and sampling

The studied limekiln (latitude 40°55′24.3″N, longitude 3°48′30.9″W) is located within the archaeological sites of Pinilla del Valle (1104 m a.s.l., Madrid, central Spain). This is a middle Palaeolithic complex where several sites are in the process of being excavated. It is located in the upper valley of the Lozoya river in the Sierra de Guadarrama, about 90 km from the city of Madrid, in a mountainous area that is part of the Iberian Central Range System (Fig. 1). Systematic archaeological excavations have been carried out since 2002 and an outstanding middle Palaeolithic archaeo-palaeontological record associated with *Homo neanderthalensis* remains has been discovered (e.g., Márquez *et al.* 2013). During the 2008 season, the limekiln was discovered and excavated. The position of the limekiln inside the Palaeolithic complex is merely coincidental. It was constructed by excavating a cavity inside the clay deposits that are part of the Palaeolithic complex. However, there is no evident archaeological (cultural) relationship between them.

The studied limekiln is cylindrical (3 m in height and 1.8 m in diameter) and it is well preserved (Fig. 1). A limekiln is a type of kiln the main function of which is to obtain calcium oxide (CaO), commonly known as lime, through the calcination of limestone at elevated temperatures, usually above 900 °C (Senegacnik *et al*. 2007). Lime production has been a well-documented process since Roman times (e.g., Donadini *et al*. 2010; Ventolà *et al*. 2012), with applications such as masonry works or even disinfectant, among others.

During the excavation of the limekiln, abundant ashes, charcoal remains and other debris were extracted, but no archaeological remains representative of the time of its abandonment (e.g.,

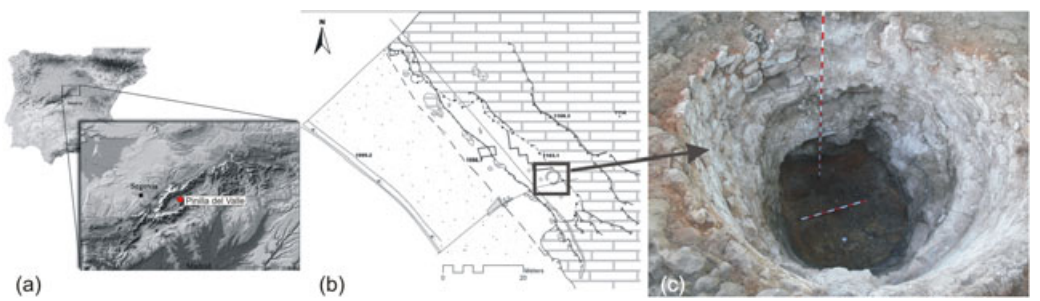

Figure 1 *(a) Maps showing the location of Pinilla del Valle sites. (b) A plan view of the sites, showing the exact location of the limekiln studied, which is amplified in (c). Horizontal bar for scale: 1 m.*

pottery) were found. Other limekilns are documented in the surrounding area, a few kilometres away. Although it is known, from oral testimonies, that some of them were in use until the mid-20th century (Mazadiego *et al.* 2005), none of them has been radiometrically dated so far. The limekiln studied here is difficult to date based on archaeological evidence because of its uncertain association with other archaeological features. The foundation of certain local villages such as Rascafría goes back to late medieval times, its name first being cited in a document of 1390. Also dating from this period is the local Carthusian monastery of El Paular, close to which the existence of a limekiln has been known since the mid-18th century (cf., Jiménez de Gregorio 1990). The only references to the lime from this period are indirect. Mazadiego *et al.* (2005) make reference to several historical documents of the past three centuries, where it is stated that houses were built with granite blocks embedded using a mortar made of lime and sand. This provides evidence that lime production played an important role, but it is still the case that nothing is known about the age of the last use of this limekiln.

Thirty-two oriented cylindrical cores (samples) were collected from the internal wall of the limekiln at different heights, starting from the lower part and proceeding up to the top. Sampling was performed using a portable electrical drill, which incorporates a water-cooled diamond bit. The azimuth and dip of each core were measured with a magnetic compass and an inclinometer, following the standard palaeomagnetic sampling procedure. The compass readings were corrected by the local declination of the site. Twenty-five cores produced a single specimen, while from the rest seven cores, two specimens per sample, were obtained (labelled 'b' in Table 1 below). After subsampling, a total of 39 specimens were obtained and measured. The studied lithologies correspond to baked clays (eight samples—eight specimens), limestones (17 samples—23 specimens), sandstones (four samples—five specimens) and an isolated slab of foidite, an igneous material (three samples—three specimens), all showing evidence of having experienced high temperatures during heating (e.g., whitish coatings indicative of calcination). Small fragments of representative samples from each lithology were used for rock-magnetic and palaeointensity analysis. The dominant material used for the construction of the limekiln is a local Upper Cretaceous limestone, although other lithologies are also present. There is no preferential use of materials depending on the height of the limekiln. Baked clays are more abundant at the base, but not exclusively, and their thickness is variable, they are sometimes absent while in other cases they reach 4–5 cm. They probably correspond to the substrate in which the limekiln was built. The slab of foidite appears in the upper part of the limekiln, and considering that igneous rocks are also documented in this region (Karampaglidis *et al.* 2015), its presence is not so strange. However, the reason why it only appears as an isolated block is unknown.

Magnetic methods

Archaeomagnetic (directional) and rock-magnetic analyses were carried out at the Laboratory of Palaeomagnetism of Burgos University (Spain). Archaeointensity determinations were performed in the palaeomagnetic laboratory of the National University of Mexico, (UNAM, Campus Morelia, Mexico). Directional analysis comprised the stepwise demagnetization of the natural remanent magnetization (NRM) by alternating field (AF) or thermal (TH) demagnetization and its measurement with a 2G SQUID magnetometer (noise level $\sim 5 \times 10^{-12}$ A m^2). AF demagnetization was carried out in 20 steps up to a maximum peak field of 100 mT with the 2G magnetometer. Thermal demagnetization was performed in 15 steps up to 585 °C using a TD48-SC (ASC) thermal demagnetizer. Low-field magnetic susceptibility (MS) was measured

Table 1 *The directional results of the Pinilla del Valle limekiln (latitude 40°55'N, longitude 3°48'W)*

Sample	*Specimen code*	*Declination, D (degrees)*	*Inclination, I (degrees)*	*Koenigsberger ratio, Q_n*	*Maximum angular deviation (MAD)*[*]	*ChRM*[†]	*Lithology*
CP01	CP01a	356.3	40.3	11.4	1.0	15–80 = mT	Baked clay
CP02	CP02a	5.2	42.4	8.7	0.6	15–60 mT	Baked clay
CP04	CP04a	9.2	38.2	2.8	4.4	250–580 °C	Baked clay
CP05	CP05a	354.4	47.0	6.1	1.1	250–580 °C	Baked clay
CP06	CP06a	8.4	51.8	6.7	1.0	250–580 °C	Baked clay
CP07	CP07a	1.9	50.2	15.1	2.3	275–580 °C	Baked clay
CP08	CP08a	0.7	50.8	8.3	0.5	15–100 mT	Baked clay
CP09	CP09a	357.5	52.0	6.6	1.7	250–580 °C	Limestone
CP11	CP11a	355.8	32.7	10.4	1.3	250–580 °C	Limestone
CP12	CP12a	8.64	40.1	9.1	0.6	15–100 mT	Limestone
CP13	CP13a	358.9	46.1	21.2	0.5	15–100 mT	Limestone
	CP13b‡	359.7	41.1	10.2	1.1	275–580 °C	Limestone
	Mean CP13a–b	359.3	43.6				
CP14	CP14a	3.0	42.6	19.9	0.6	250–580 °C	Limestone
CP15	CP15a	6.5	40.5	0.5	0.7	15–100 mT	Limestone
CP16	CP16a	3.0	44.1	2.4	0.8	250–580 °C	Limestone
CP17	CP17a	355.5	47.5	7.5	0.7	250–580 °C	Limestone
	CP17b	3.3	43.0	11.2	0.2	15–100 mT	Limestone
	Mean CP17a–b	359.6	45.4				
CP18	CP18a	0.4	46.9	7.3	1.7	250–580 °C	Limestone
	CP18b	356.7	45.9	10.3	0.4	15–100 mT	Limestone
	Mean CP18a–b	358.6	46.5				
CP19	CP19a	353.6	44.1	3.7	0.9	250–580 °C	Limestone
	CP19b	356.4	43.1	9.9	0.5	15–100 mT	Limestone
	Mean CP19a–b	355.0	43.6				
CP22	CP22a	18.0	35.7	6.8	3.5	250–580 °C	Sandstone
CP24	CP24a	352.0	40.9	8.6	1.2	250–580 °C	Sandstone
	CP24b	353.7	39.3	6.9	0.4	15–100 mT	Sandstone
	Mean CP24a–b	352.9	40.1				

(*Continues*)

Table 1 *(Continued)*

Sample	*Specimen code*	*Declination, D (degrees)*	*Inclination, I (degrees)*	*Koenigsberger ratio, Q_n*	*Maximum angular deviation (MAD)*[*]	*ChRM*[†]	*Lithology*
CP25	CP25a	7.4	45.4	5.8	1.2	250–580 °C	Limestone
CP27	CP27a	357.8	48.6	13.5	0.8	300–580 °C	Limestone
	CP27b	357.1	49.9	11.5	1.3	250–580 °C	Limestone
	Mean CP27a–b	357.5	49.2				
CP29	CP29a	359.9	47.2	18.3	1.9	250–580 °C	Sandstone
CP30	CP30a	10.0	46.9	7.8	0.8	250–580 °C	Limestone
CP32	CP32a	2.2	41.8	3.7	1.4	250–580 °C	Limestone
Mean direction at sample level§		D_m (degrees)	I_m (degrees)	k	α_{95}	N/N'	
		2.2	44.3	147.3	2.4	24/32	

[*]Kirschvink (1980).

[†]The interval of the NRM demagnetization sequence considered to calculate the characteristic remanent magnetization direction.

[‡]The six specimens labelled 'b' refer to double specimens obtained from the same core (sandstone specimen CP22b was excluded due to incomplete isolation of the ChRM component).

§D_m and I_m are the mean declination and inclination, calculated at sample level; k and α_{95} are the precision parameter and the 95% confidence limit of the ChRM, from Fisher's (1953) statistics; N/N´ is the number of samples considered to compute the mean direction divided by the number of independently oriented samples collected.

initially and after each thermal demagnetization step with a Kappabridge KLY-4 (AGICO, noise level 3×10^{-8} S.I.) to evaluate possible magneto-chemical alterations during heating. The characteristic remanent magnetization (ChRM) direction for each sample was calculated by linear regression, including at least six demagnetization steps. Mean directions and associated statistical parameters were calculated using Fisher (1953) statistics.

In order to characterize the magnetic remanence carriers and their domain state, a set of rock-magnetic experiments was undertaken. These techniques are widely used in rock- palaeo- and environmental magnetic studies and will not be described here. For detailed information, the reader is referred to textbooks (Dunlop and Özdemir 1997; Tauxe *et al.* 2010). With a Variable Field Translation Balance (MM_VFTB), we measured progressive isothermal remanent magnetization (IRM) acquisition curves, hysteresis loops (± 1 T), backfield coercivity curves and thermomagnetic curves (magnetization versus temperature) up to 700 °C in air. These analyses were carried out on bulk samples (~ 450 mg) from 23 representative specimens. The results from the hysteresis and backfield curves were interpreted using the RockMagAnalyzer 1.0 software (Leonhardt 2006). The saturation magnetization (M_s), remanence saturation magnetization (M_{rs}) and coercive field (B_c) were calculated from hysteresis loops after subtracting the paramagnetic contribution. These parameters combined with the coercivity of remanence (B_{cr}), obtained independently from the backfield curves, allowed us to estimate the domain state distribution of the samples in the Day plot (Day *et al*. 1977; Dunlop 2002). The Curie temperatures were estimated from the thermomagnetic curves using the two-tangent method of Grommé *et al*. (1969). Additionally, representative samples were also selected to carry out thermal demagnetization of the IRM in three orthogonal axes, following Lowrie's (1990) method. The applied fields were 2 T, 0.4 T and 0.12 T for the *Z*-, *X*- and *Y*-axes, respectively. Thermal demagnetization was performed in 16 temperature steps distributed between room temperature and 700 °C.

Twenty-four specimens from 11 independent samples were selected for absolute intensity measurements based on their stable thermomagnetic behaviour and relatively high NRM. The Thellier–Coe type experiments (Thellier and Thellier 1959; Coe 1967) were carried out using an ASC Scientific TD48-SC furnace; all heating/cooling runs were performed in air. Eleven temperature steps were distributed from 100 to 540 °C, with reproducibility between two heating runs to the same nominal temperature better than 2 °C. The laboratory field strength was set to (50.0 ± 0.05) μT. Partial thermoremanent magnetization reinvestigations (pTRM checks) at each third temperature step were added to the protocol.

The acceptance criteria for individual palaeo- or archaeointensity determinations are now mostly standardized and may be summarized as follows. (1) Directions of NRM end-points at each step obtained from Thellier double heating experiments have to fall along a straight line, trending towards the origin in the interval chosen for archaeointensity determination. (2) No significant deviation of NRM directions towards the applied field direction should be observed. (3) At least five aligned TRM–NRM points on the Arai plot must be used (specimens suspected to carry considerable viscous remanent magnetization acquired *in situ* are rejected). (4) The NRM fraction factor (*f*, Coe *et al*. 1978) ≥ 0.3. This means that at least 30% of the initial NRM was used for archaeointensity determination. (5) A quality factor (Coe *et al*. 1978) $q \geq 4$ (generally above 5), being $(f^* g)/\beta$, where g is the gap factor (Coe *et al*. 1978) and β is the relative standard deviation of the slope. (6) Archaeointensity results obtained from NRM–pTRM diagrams must not show an evident concave-up shape, since in such cases remanence is probably associated with the presence of MD grains (Levi 1977; Kosterov *et al*. 1998). (7) There must be positive pTRM checks; that is, the deviation of the 'pTRM' checks must be less than 15%.

RESULTS

Rock magnetism

Initial NRM intensity and low-field MS values vary between 8.91×10^{-3} A m^2 kg^{-1} and 5.47×10^{-7} A m^2 kg^{-1} and between 9.52×10^{-6} m^3 kg^{-1} and 5.82×10^{-9} m^3 kg^{-1}, respectively. The highest NRM and MS values correspond to the foidite and baked clays and the lowest values to sandstones and limestones, the latter two being quite variable. Figure 2 shows the Koenigsberger ratio [Q_n = NRM/(χH) (cf., Stacey 1967)], where χ is the magnetic susceptibility and H is the local geomagnetic field strength. This parameter is based on the relationship between the induced and the remanent magnetization, and provides an estimate of the efficiency of NRM acquisition mechanism. With the exception of a limestone sample (CP15a = 0.52), all values are higher than unity, oscillating between 2.42 and 72.8 (Fig. 2), indicating a thermoremanent origin of the NRM.

The majority of progressive IRM acquisition curves are almost saturated between 150 and 300 mT, indicating that the remanent magnetization is dominated by low-coercivity minerals (magnetite and/or maghemite). However, some samples do not reach complete saturation even at 1 T (the maximum field applied), pointing out that a small fraction of high coercivity is also present (Fig. 3).

The hysteresis ratios range from $0.065 < M_{rs}/M_s < 0.468$ and $1.399 < B_{cr}/B_c < 3.593$, showing the dominance of pseudo-single domain (PSD) particles in the assemblage (Fig. 4). Data comparison with the theoretical mixing lines of Dunlop (2002) shows some granulometric differences among lithologies. Most samples plot closer to the single-domain (SD) region, which is more appropriate for absolute palaeointensity analysis. Limestone (the most sampled lithology) and baked clays dominate the plot and only few samples of the other lithologies could be measured because there was no remaining sample after carrying out directional analyses. Baked clays are well clustered in the central PSD region, pointing to slightly coarser grain sizes than limestones, which display a higher M_{rs}/M_s ratio and lower B_{cr}/B_c values

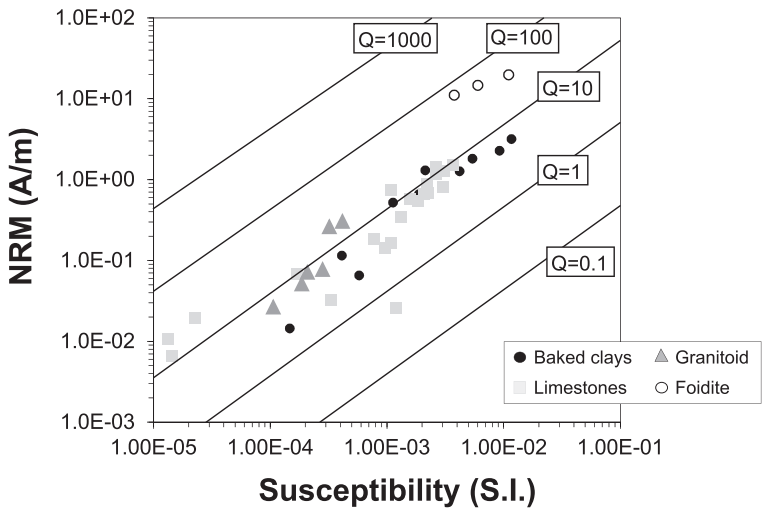

Figure 2 *The natural remanent magnetization (NRM) versus the bulk magnetic susceptibility (S.I.), showing lines of constant Koenigsberger ratio (Q_n) between 0.1 and 100.*

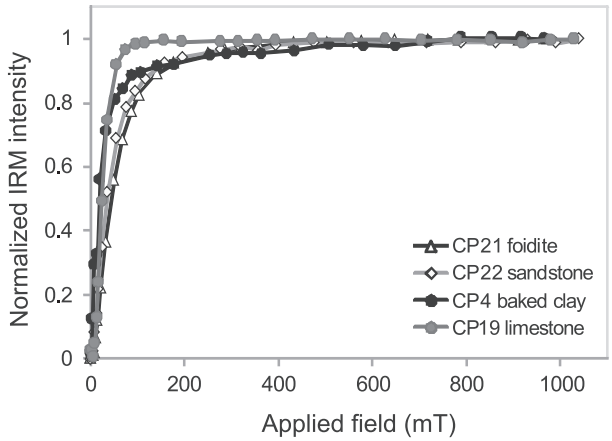

Figure 3 *Progressive isothermal remanent magnetization (IRM) acquisition curves up to 1 T for representative samples.*

(more SD-like) than baked clays. Sandstones show similar behaviour, but with significantly lower B_{cr}/B_c values than baked clays. In general, B_{cr}/B_c ratios display lower values than those predicted by Dunlop (2002) in similar materials, but they all fall within the expected range. Foidite data are more dispersed, with one sample very close to the SD region and two others very similar to baked clays. According to the mixing curves of Dunlop (2002), the contribution of the finest superparamagnetic (SP) particles seems to be more significant in baked clays and some limestones.

As far as the mineralogical composition is concerned, the thermomagnetic curves are quite heterogeneous (Fig. 5). In general, the heating and cooling curves are not fully reversible, suggesting that mineralogical changes occurred during heating. All curves contain a phase with a Curie temperature (T_C) ~ 585 °C, indicating that Ti-low titanomagnetite is the main magnetic carrier. This single phase has been observed mainly in baked clays (Fig. 5 (a)) but also in some limestones (Figs 5 (b) and 5 (c)). Some limestones exhibit a high degree of thermomagnetic reversibility (Fig. 5 (c)) indicating that they are thermally stable. In other cases (two samples), a characteristic hyperbolic shape is observed (Fig. 5 (d)), probably due to a strong paramagnetic contribution. Interestingly, the concentration of ferromagnetic minerals in limestones is rather variable, since their intensity of magnetization varies up to three orders of magnitude. Apart from the magnetite phase, a slope change at intermediate temperatures (~250 °C) is also observed in the heating cycle of Figure 5 (f), probably due to maghemite inverting to less magnetic hematite during heating. A subtle inflection over 600 °C in the sandstone sample (Fig. 5 (e)), suggests that hematite is also present.

Thermal demagnetization of the three orthogonal components of the composite IRMs provide information on the remanence carriers and their relative contribution to the magnetization. The intensity of magnetization in all samples is dominated by the low-coercivity component ($\leq$ 0.12 T), with a maximum unblocking temperature (T_{UB}) of ~580–600 °C indicating the presence of a spinel phase of near-magnetite composition (Fig. 6). Some limestones (Fig. 6 (c)) and sandstones (Fig. 6 (d)), show a maximum T_{UB} of 675–700 °C on the high-coercivity axis ($\leq$ 2 T), indicating that hematite is also present, although with a tiny remanence contribution. The contribution of the intermedium coercivity axis ($\leq$ 0.4 T) to the remanence is not significant for all lithologies.

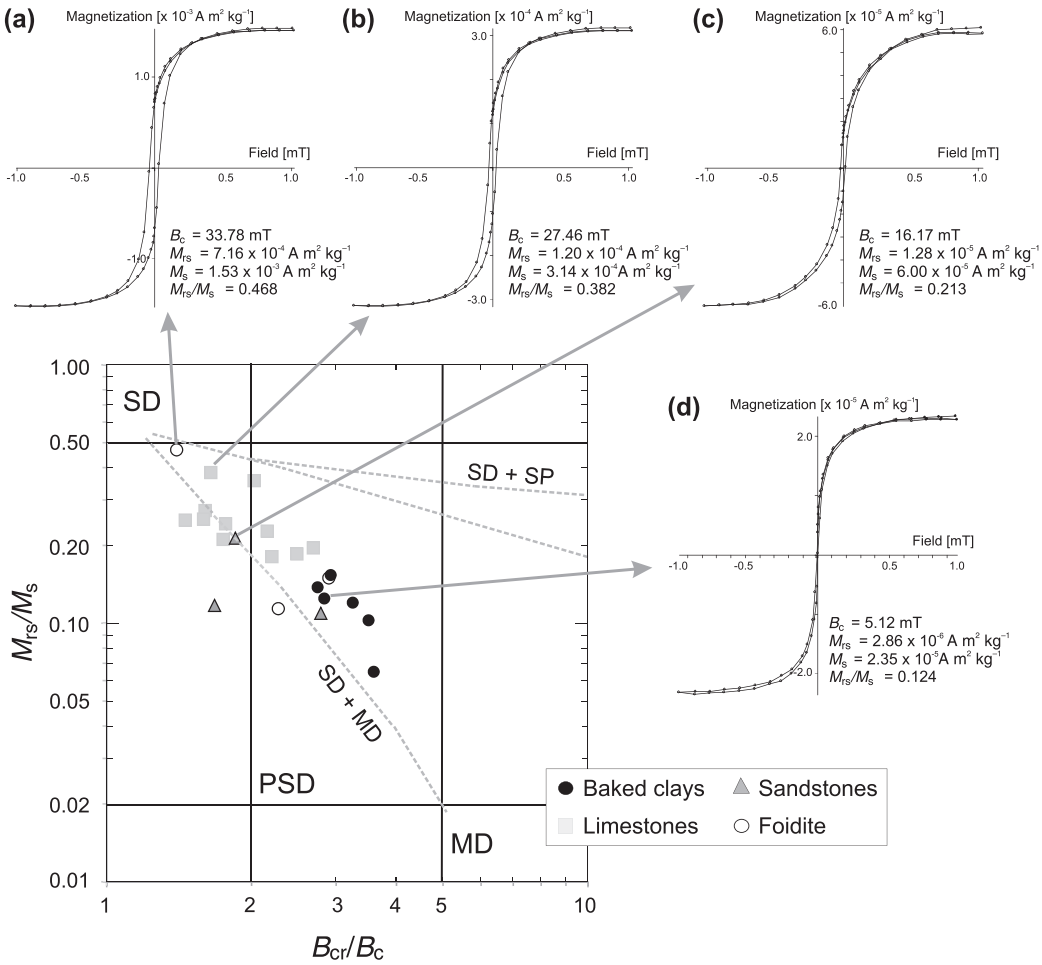

Figure 4 *M_{rs}/M_s versus B_{cr}/B_c logarithmic plot of various samples: the dashed lines represent mixing curves taken from Dunlop (2002) for mixtures of single-domain (SD) with multi-domain (MD) or superparamagnetic (SP) magnetite particles. (a–d) Four examples of hysteresis loops—(a) CP31, foidite, (b) CP11, limestone, (c) CP24, sandstone and (d) CP4, baked clay—with their respective hysteresis parameters.*

To sum up, considering that most IRM acquisition curves are almost saturated at 300 mT, the low B_c (4.2–33.7 mT) and B_{cr} (14.5–47.2 mT) values obtained, the maximum T_{UB} of ~585–600 °C on the dominant low-coercivity axis (3IRM tests) and the T_c of about 580 °C point to magnetite with a low degree of isomorphous substitution as the main magnetic carrier. Furthermore, the hysteresis results suggest an important contribution of PSD–SD grains carrying a stable magnetic signal.

Archaeomagnetic direction

Representative examples of NRM orthogonal demagnetization diagrams are shown in Figure 7, together with their respective normalized decay intensity curves and a stereographic projection

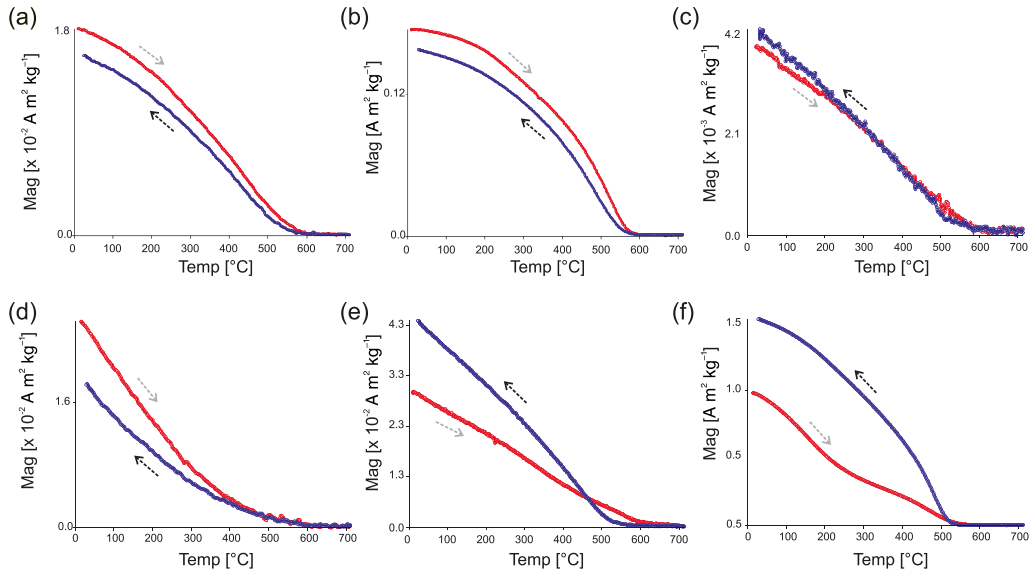

Figure 5 *Representative thermomagnetic curves (J versus T): (a) CP4–1 (baked clay); (b) CP34 (limestone); (c) CP14_2 (limestone); (d) CP15 (limestone); (e) CP24 (sandstone); (f) CP31 (foidite). Heating (cooling) cycles are plotted in red (blue) with their respective arrows. The sample code, lithology and intensity of magnetization are indicated for each sample.*

with the ChRM directions at sample level considered to calculate the mean direction. Directional results used to compute the ChRM directions as well as the mean direction calculated at sample level are also shown in Table 1. Three specimens from the foidite slab with the highest NRM intensity values (between 19 and 11 A m^{-1}) were rejected due to inconsistent archaeomagnetic directions and another five (a baked clay, three limestones and a sandstone) were also rejected due to incomplete isolation of the ChRM component or a poorly defined demagnetization path. Another limestone specimen broke during demagnetization.

In general, the NRM directional stability is very reproducible among samples of different lithologies and both AF (Figs 7 (a) and 7 (b)) and TH demagnetization produced similar results (Figs 7 (c) – 7 (e)). Below 250 °C or 15 mT, the NRM is mostly unstable, probably due to viscous component contributions. However, after 15 mT, the NRM stability in AF samples is defined by a stable single component that is almost demagnetized at 100 mT (Fig. 7 (a)), indicating that the dominant NRM carrier is a low-coercivity mineral. The only exception is a limestone specimen (Fig. 7 (b)) with almost 20% of the initial NRM remaining at 100 mT (see the decay intensity curve) due to the contribution of a high-coercivity mineral, most probably hematite. In any case, the ChRM direction has been successfully isolated here.

The TH demagnetized samples also exhibit a well-defined, high-intensity stable component and the ChRM direction was calculated from 250–300 °C to 585 °C (Figs 7 (c) – 7 (e)). The decay intensity curves confirm that most of the magnetization is lost during heating between 400 and 585 °C, pointing to Ti-low titanomagnetite as the carrier of the magnetization. The low-field MS measured after each TH demagnetization step (not shown here) exhibited very little variation for the entire collection, so no significant mineralogical transformations took place during the thermal demagnetization. The ChRM component isolated by AF or TH demagnetization

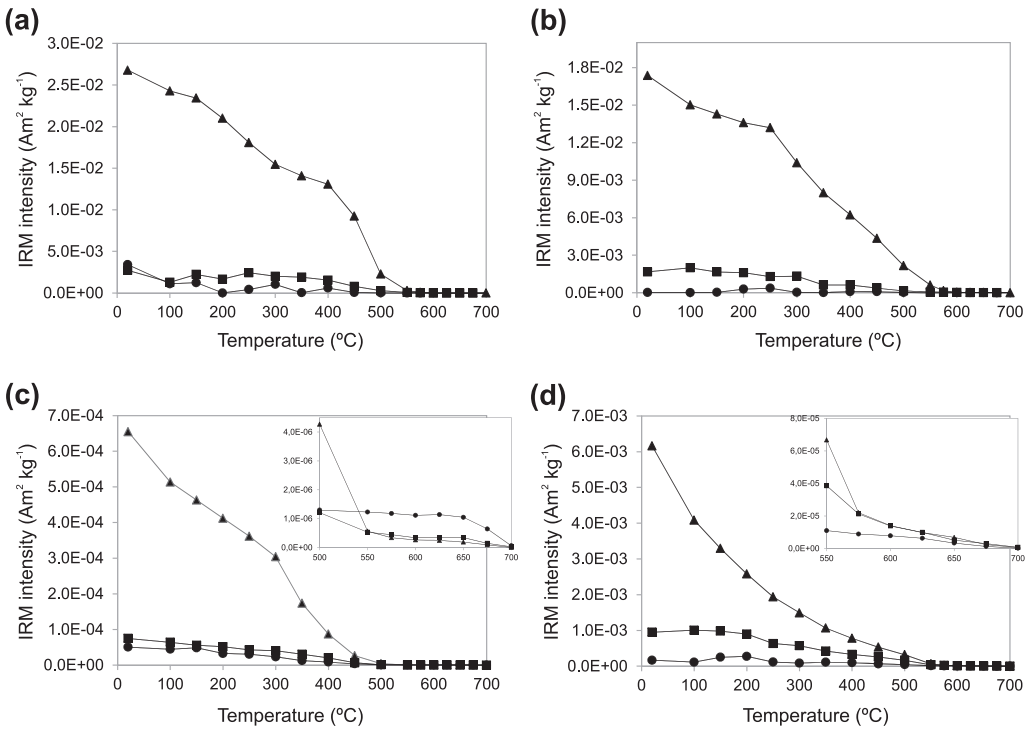

Figure 6 *Examples of stepwise thermal demagnetization of composite IRMs (cf., Lowrie 1990): (a) CP5 (baked clay); (b) CP12 (limestone); (c) CP15 (limestone); (d) CP23 (sandstone). The high (2 T), intermediate (0.4 T) and low-coercivity (0.12 T) components are denoted with circles, squares and triangles, respectively. The higher-temperature steps in panels (c) and (d) are blown up to show the presence of hematite.*

yielded directions similar to those of the stereographic projection shows (Fig. 7 (f)). The well-defined mean archaeomagnetic direction obtained (Dec. = 2.2°; Inc. = 44.3°; $k = 147.3$; $\alpha_{95} = 2.4°$) was successfully determined on 24 samples (Table 1) and characterized by high-precision parameters (k) and low semi-angles of confidence (α_{95}) according to Fisher's (1953) statistics. Taking into account the consistent NRM directional stability, the high Q_n ratios obtained (also for specimens 'b' in Table 1) and the rock-magnetic results reported before, the component considered as the ChRM direction is most probably related to a TRM acquired during the last heating and subsequent cooling of the structure.

Determinations of the absolute archaeointensity

The intensity of the thermoremanent magnetization of a sample is related to the cooling rate (e.g., McClelland-Brown 1984). Whereas the time of cooling of the samples in the laboratory from high temperature (~570 °C) to room temperature varied between 30 and 45 min, depending on the furnace, the time of the original (last) cooling of limekiln can be much longer (Genevey and Gallet 2003; Morales *et al*. 2011). For this reason, the correction by cooling rate is a critical factor when obtaining reliable ancient intensities. The dependency of the TRM with the cooling rate was investigated following a modified version of the procedure

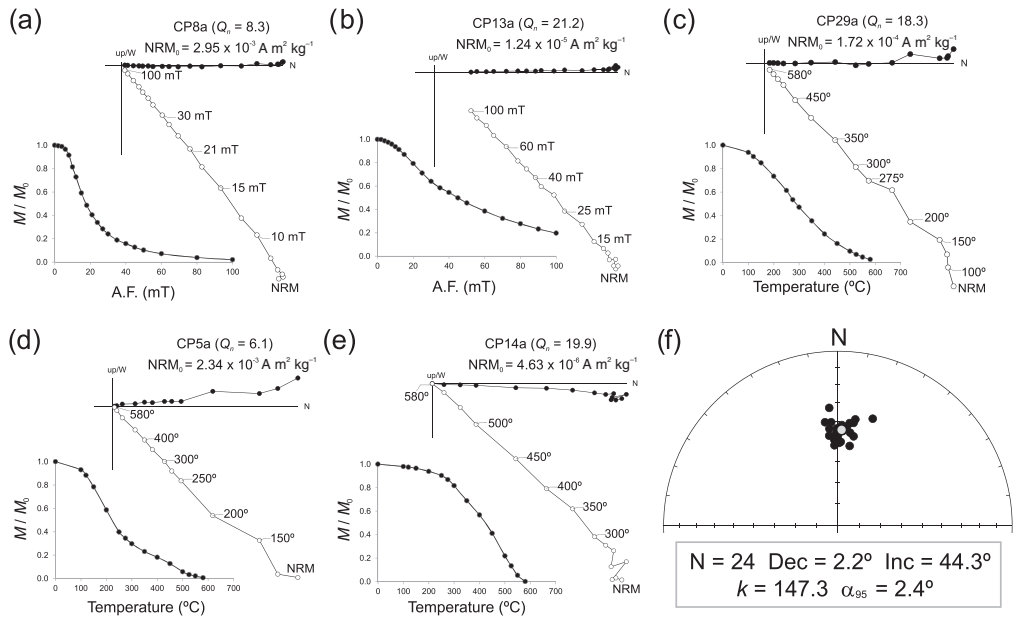

Figure 7 *Representative orthogonal NRM demagnetization plots. Open (closed) symbols represent the vertical (horizontal) projections of vector endpoints. The sample code, intensity (NRM_0), Koenigsberger (Q_n) ratio and normalized demagnetization spectra are shown for each sample. (a,b) AF, alternating field; (c–e) TH, thermal. (f) An equal-area projection of all ChRM directions, with the mean direction calculated at sample level and the α_{95} confidence circle (in grey). N, number of samples; Dec., declination; Inc., inclination; k, precision parameter; α_{95}, semi-angle of confidence.*

described by Chauvin *et al*. (2000). The commonly used anisotropy correction requires at least six additional heatings at high temperature, when usually less than 15% of the original magnetization survives, which may alter the original TRM. To try to overcome these circumstances, we use a protocol that, at least experimentally, has proved to be a good alternative. Each sample was arbitrarily marked in six positions (± *X*, *Y*, *Z*) with parallel arrows on its internal or external flattening plane to create a reference orientation. Samples were then embedded in ultra-pure salt (NaCl) pellets, compressed with a non-magnetic hydraulic press in order to treat them as standard palaeomagnetic cores. This allows us to overcome the possible bias due to remanence anisotropy and to decrease the number of heatings, which may significantly alter the magnetic mineralogy of the samples. This was experimentally proved by our numerous published (e.g., Morales *et al.* 2009; Goguitchaichvili *et al.* 2015) and unpublished works measuring laboratory-simulated TRM aquisitions under a controlled (present-day) field and atmosphere. It is also true that this approach may increase the internal dispersion of absolute intensity.

Some representative determinations are shown in Figures 8 (a) – 8 (c), where all the criteria quoted above are fulfilled: the Arai plots and Zijderveld diagrams are linear, the NRM end directions point to the origin and the pTRM checks are positive (within the limits defined above). A small secondary viscous component is present in some cases, but it is generally removed at low temperatures, around 250 °C. Samples with Coe quality factors lower than those defined by the acceptance criteria and poor alignment of NRM–TRM points have not been taken into consideration for the calculation of the kiln's mean value.

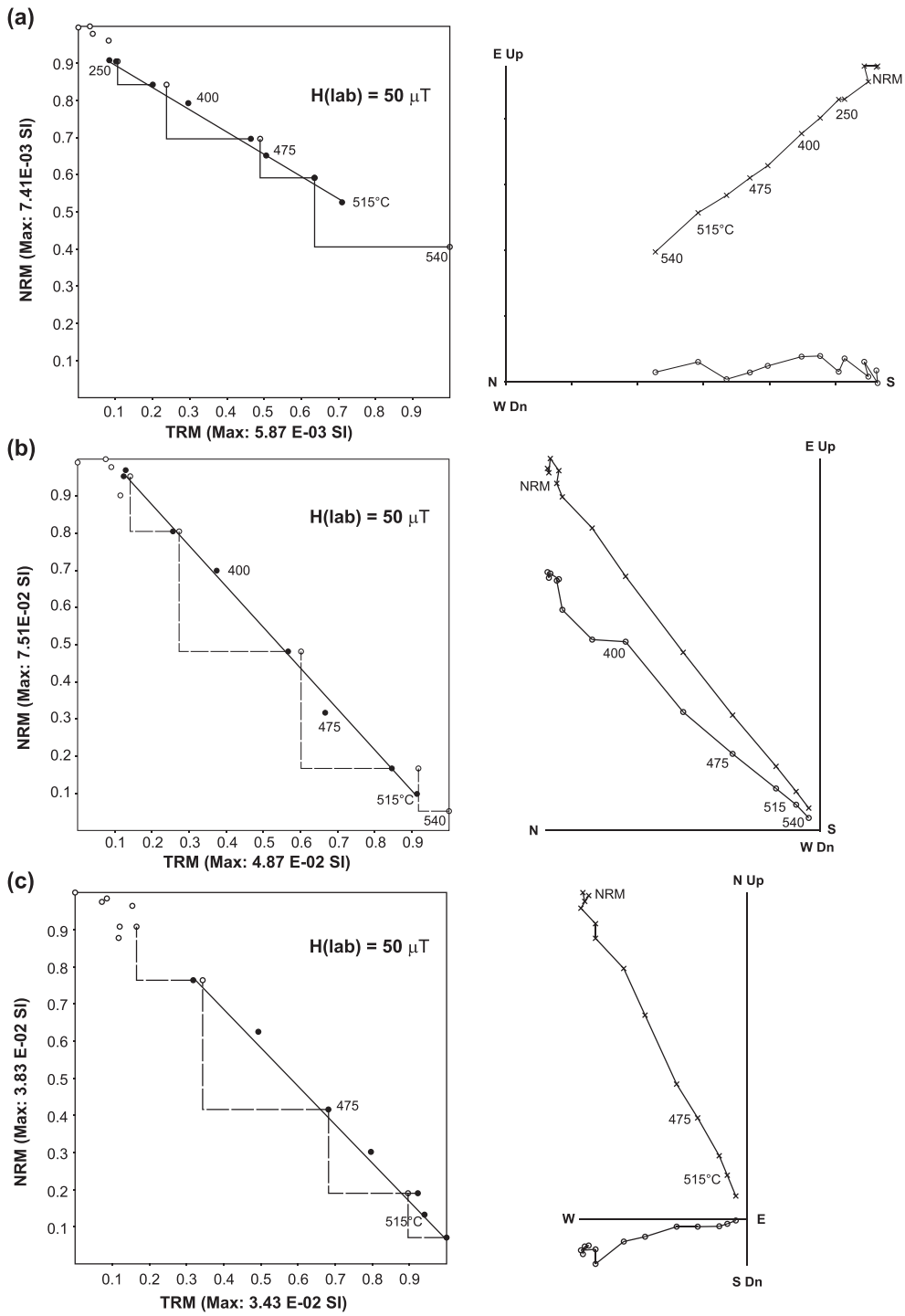

Figure 8 *Representative NRM–TRM plots (so-called Arai–Nagata plots) and associated orthogonal vector demagnetization diagrams for representative samples: (a) sample 23B-2; (b) sample 30B-1; (c) sample 32B-1.*

In summary, 11 out of 24 analysed specimens yield reliable absolute intensity determinations (Table 2). For these specimens, the NRM fraction *f* used for determination ranges between 0.82 and 0.43 and the quality factor *q* from 4.8 to 23.1, being generally greater than 5. We accepted a lower *q* value in a single case (specimen 32B-1) because the corresponding intensity (49.4 μT) was very close to the site's mean value (43.8 ± 7.69 μT).

DISCUSSION

The mean directional and intensity values obtained were compared with the SCHA.DIF.3 K model (Pavón-Carrasco *et al*. 2009). This model describes the variation of the three geomagnetic field elements in Europe for the past 3000 years at the site coordinates, thus avoiding any relocation error (Casas and Incoronato 2007). Archaeomagnetic dating of the limekiln was carried out using the MATLAB® dating tool of Pavón-Carrasco *et al*. (2011), and the probability density functions of possible dates obtained for directional and intensity geomagnetic parameters at the 95% probability level are shown in Figure 9.

As far as the declination is concerned, up to four different possible dating intervals result for the past 2000 years: the mid-first to the early third century AD, the early fourth to the end of the sixth century AD, the mid-13th to the early 16th century AD, and the 17th century AD. In contrast, when inclination is considered, only one dating interval is obtained (the end of the 12th to the early 15th century AD), constraining the last use of the limekiln much more significantly. The archaeointensity mean value is not particularly helpful here because, despite the good quality of the data, their associated statistic is poor (a high uncertainty band) and four wide dating intervals are obtained: the first century AD, the mid-second to the end of the third century AD, the mid-fourth to the early eighth century AD, and from the mid-10th century onwards. Combination of the probability density functions of all elements calculated at the 95% confidence interval yields a date for the last use of the kiln of AD 1296–1413.

Table 2 *Archaeointensity results at specimen level, where $T_{min} - T_{max}$ is the temperature interval of intensity determination, n is the number of heating steps used for the intensity determination, f is the fraction of NRM used for intensity determination, g is the gap factor, q is the quality factor as defined by Coe et al. (1978) and H_{corr} is the archaeointensity value corrected for cooling rate effect. The final mean intensity value was calculated excluding two limestone specimens (30B-1 and 30B-2)—see the text for an explanation*

Lithology	*Specimen*	*n*	$T_{min} - T_{max}$ (°C)	*σH*	*f*	*g*	*q*	H_{corr} (μT)
Baked clay	7 A-1	6	250–500	1.1	0.59	0.74	11.4	36.5
Baked clay	7 A-2	8	250–540	1.6	0.66	0.84	12.8	48.2
Limestone	12B-1	7	250–515	3.6	0.71	0.79	7.9	50.1
Limestone	12B-2	7	250–515	4.8	0.73	0.79	7.4	52.6
Sandstone	23B-1	7	300–540	0.8	0.62	0.81	7.3	35.6
Sandstone	23B-2	7	250–515	1.4	0.43	0.83	7.8	36.6
Sandstone	29B	7	300–540	0.5	0.61	0.80	12.7	34.4
Limestone	30B-1	10	200–540	4.1	0.82	0.83	23.1	79.5
Limestone	30B-2	9	250–540	2.5	0.76	0.82	16.7	74.5
Limestone	32B-1	6	250–500	4.1	0.49	0.75	4.8	49.4
Limestone	32B-2	7	300–540	3.6	0.75	0.82	8.4	50.5
Mean intensity								43.8 ± 7,69 μT

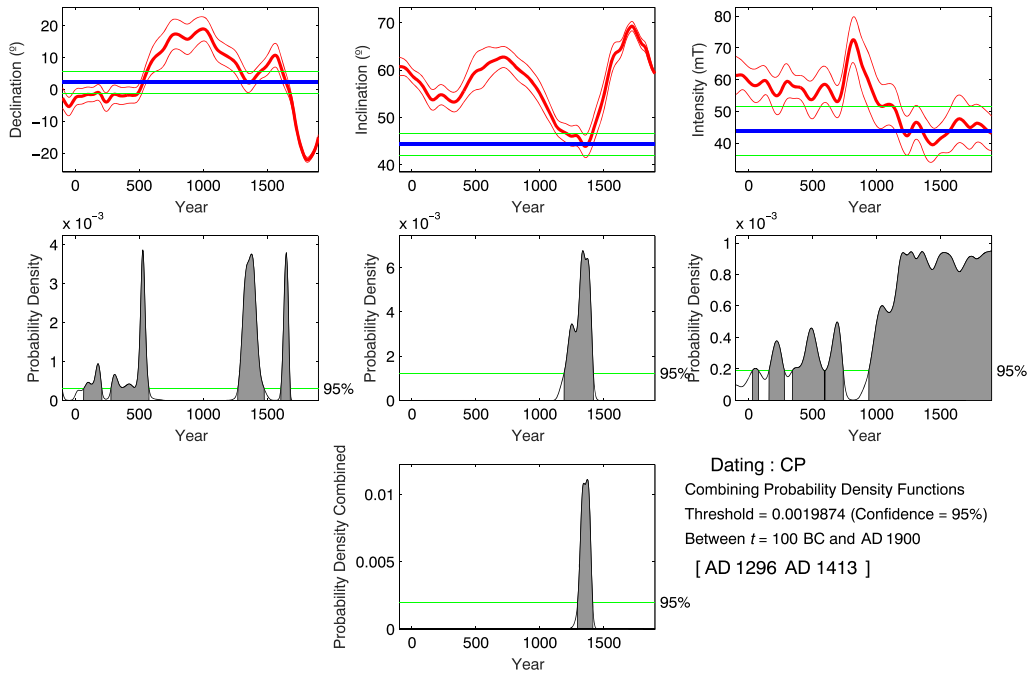

Figure 9 *Probability-of-age density functions obtained with the MATLAB tool from Pavón-Carrasco et al. (2011) for declination, inclination and intensity values using the SCHA.DIF.3 K model.*

Archaeomagnetic dating can be reliably interpreted only when associated with a chronological context provided by absolute dating methods and/or archaeological evidence (e.g., decorated pottery, stratigraphy etc). In this case, two accelerator mass spectrometry (AMS) radiocarbon determinations, obtained from two different charcoal fragments and analysed in two different laboratories, agree very well with the archaeomagnetic dating interval obtained, leaving no doubt about the date of last use of the limekiln. The first date (Beta Analytic Inc.) yields an age of 640 ± 40 yr. BP (1282–1399 cal AD) and the second one (Groningen University) is 705 ± 25 yr. BP (1263 1381 cal AD), both being calibrated using the CALIB REV 7.0.2 program (Reimer *et al*. 2013) and expressed at 2δ range. According to archaeomagnetism, the last use of the limekiln would be slightly later than indicated by the radiocarbon dates. It should be noted that radiocarbon dating focuses on organic material associated with the structure, but not on the structure itself, as is the case with archaeomagnetic dating. In any event, all of the dating intervals are in good agreement, indicating that the last use of the limekiln took place no later than the first quarter of the 15th century AD.

Archaeomagnetic dating using only the direction or the intensity is feasible and good examples have been reported (e.g., Tema *et al*. 2013). However, the use of the total field vector generally constrains the dating better, although this has not been the case in our study due to the high degree of statistical uncertainty obtained in the archaeointensity determinations. The success rate in our archaeointensity determinations is about 30%, which is common in this type of study, considering the various factors that may cause failure of the palaeointensity experiments. The material must fulfil strict methodological requirements: the NRM must be a TRM in origin, the sample must be thermally stable and not undergo mineralogical transformations during successive

heatings in the laboratory, and the ferromagnetic particles must be preferably in single-domain (SD) state (Tauxe *et al*. 2010). In this collection, two specimens were rejected due to weak remanences and 11 specimens because they showed concave Arai diagrams indicative of MD particles (e.g., Calvo *et al*. 2002). Two specimens from the same sample (CP30, limestone) yielded the highest archaeointensity values (Table 2). Although there are no rock-magnetic data available specifically from this sample, a limestone specimen collected alongside showed evidence of maghemitization, with $T_c \sim 610\,^{\circ}C$. The occurrence of maghemite in archaeomagnetic studies is considered to be a low-oxidation product carrying a chemical remanent magnetization (CRM) or a thermochemical remanent magnetization (TCRM), which would bias the outcome of the palaeointensity experiments (Kosterov *et al*. 1998). On that basis, this determination was excluded for the calculation of the mean archaeointensity value.

It is interesting to note that the apparently low mean inclination obtained is a characteristic feature of the SV in Iberia during late medieval times (13th–15th centuries AD) (Gómez-Paccard *et al*. 2006a,b), which in this case allows us to rule out the other dating intervals obtained in declination and archaeointensity, respectively. We can also exclude the possibility that the limekiln was used after the first quarter of the 15th century AD, because the Iberian SVC for the past two or three millennia never had inclination values as low as those obtained here and, consequently, there is no other possible solution. Moreover, the statistic obtained in the mean direction is very robust, leaving no doubts (Fig. 7 (f)). In order to evaluate the reliability of the results, the mean direction obtained was compared with the ARCH3K archaeomagnetic model (Korte *et al*. 2009), which covers the past three millennia, and the Iberian archaeomagnetic data set (Gómez-Paccard *et al*. 2006b) for the timespan involved (11th–17th centuries AD), taking into account both uncertainties in ages and magnetic data. The comparison of the limekiln mean direction with both the ARCH3k model (Figs 10 (a) and 10 (b)) as well as the Iberian data set (Figs 10 (c) and 10 (d)) at the site coordinates shows a very good fit. Even though the number of data available for Iberia is considerably less, both records reproduce the minimum inclination for late medieval times (14th–15th centuries AD), demonstrating that our inclination value actually displays a feature of the Earth's magnetic field.

These results provide information that is of both archaeological and geophysical interest. From the archaeological point of view, the full-vector archaeomagnetic dating reported here (confirmed by two radiocarbon dates), corroborates the archaeologists' assumption that the limekiln tradition in this region of central Spain (Sierra de Guadarrama) dates back to at least late medieval times (e.g., Mazadiego *et al*. 2005). Lime production is known in the Iberian Peninsula since Roman times (e.g., García Menárguez 2004; Porrúa Martínez 2006) and was maintained during the Islamic period (e.g., Ordinas 1995) but, to our knowledge, this is the oldest evidence from central Spain. Most authors agree with the fact that places with high densities of limekilns are related to the proximity to population centres such as small towns or villages (Mazadiego *et al*. 2005). Hence, given the widespread use of lime in masonry works and taking into account the fact that the archaeomagnetic dating obtained coincides with the foundation of several local villages (e.g., Rascafría in the 14th century AD; Mazadiego *et al.* 2005), the need to ensure lime production for these local populations with limekilns such as the one studied here was certainly relevant.

From the geomagnetic point of view, the high-quality directional and intensity data reported can be used as reference points for improving the Iberian SVC as well as for global and regional geomagnetic field models, which can in turn be used for archaeomagnetic dating. The archaeomagnetic (directional) data available in the Iberian Peninsula for the late Middle Ages are reasonably well covered, but archaeointensity determinations are still notably scarce. For the period between the 13th and 17th centuries AD, Gómez-Paccard *et al*. (2008) has reported 13

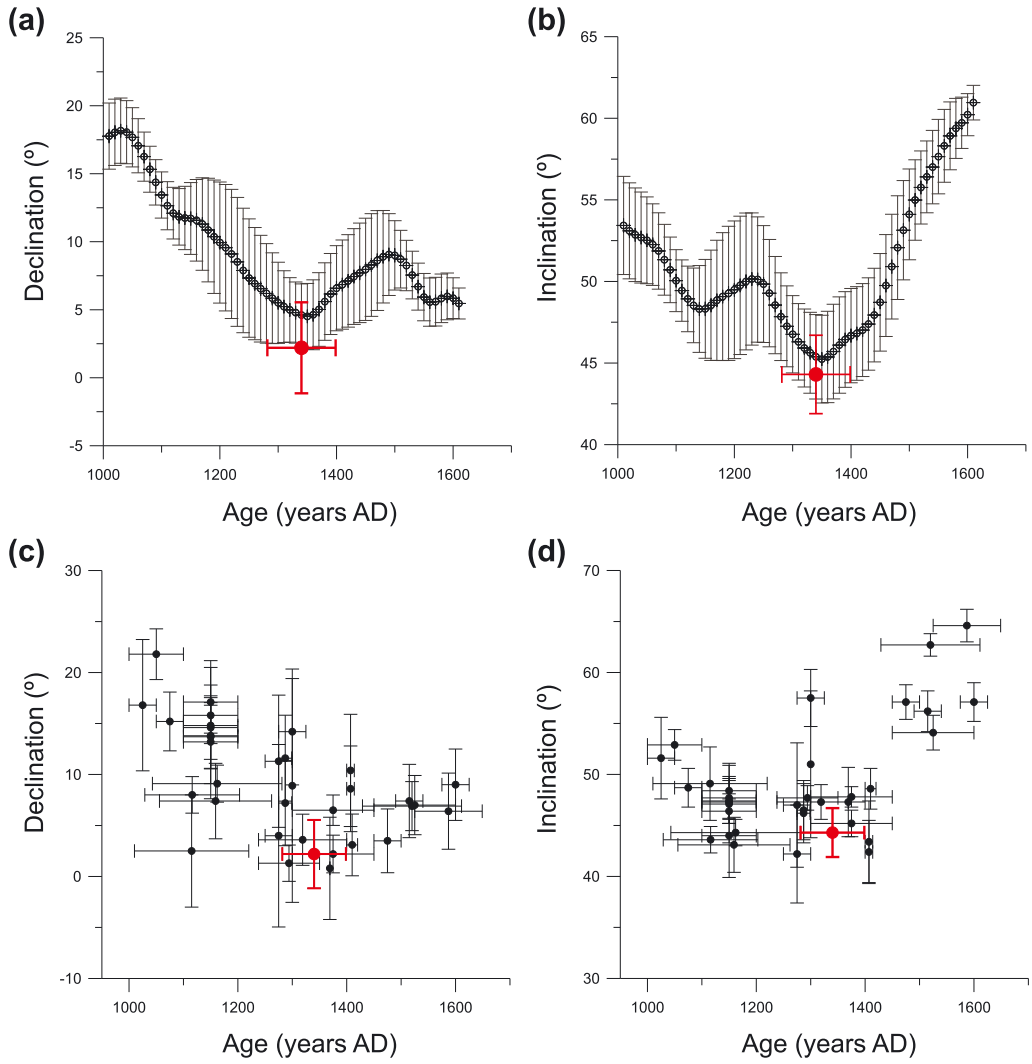

Figure 10 *Comparison of the mean directions obtained with (a,b) the archaeomagnetic model ARCH3k (Korte et al. 2009) and (c,d) the Iberian archaeomagnetic data set (Gómez-Paccard et al. 2006b) at the site coordinates. Uncertainties on ages and magnetic data are included.*

absolute archaeointensity determinations from Spain, with values ranging from 58.4 ± 3.1 μT to 47.1 ± 4.5 μT, slightly higher than ours (43.8 ± 7.69 μT) but within the error range. Yet there are still few data to define in any detail the variation of the Earth's magnetic field intensity in Iberia for this timespan. The mean direction obtained is in good agreement with model predictions and regional records (Fig. 10), and it offers more evidence about the low inclination observed in Spain around the 14th century AD. Finally, from a methodological point of view, it was not possible to obtain a directional or archaeointensity determination from the foidite in spite of its high NRM intensity. Our results suggest that such lithology should be avoided in future archaeomagnetic studies.

CONCLUSIONS

A full-vector archaeomagnetic dating has been obtained from a medieval limekiln at Pinilla del Valle archaeological site (Madrid, central Spain). The rock-magnetic results indicate the dominance of PSD–SD low-titanium titanomagnetite as the main magnetic carrier. The comparison of directional and intensity mean values obtained with the SCHA.DIF.3 K model yielded an age of last use of AD 1296–1413, in good agreement with two independent radiocarbon determinations.

Diverse dating intervals were obtained with declination and archaeointensity mean values, but the mean inclination obtained only fits with the minimum in inclination recorded in the Iberian SVC during the late Middle Ages (13th–15th centuries AD). This unequivocally allows the exclusion of any later date of last use for the limekiln. The comparison of the mean direction with the ARCH3K model and the Iberian archaeomagnetic database confirms this minimum inclination as a distinctive feature of the Earth's magnetic field. Archaeologically, the limekiln tradition in this area can be traced up to late medieval times, providing the oldest direct evidence of lime production in this region of central Spain. Alternatively, the total field vector data reported can be included as reference points into the Iberian SVC and geomagnetic field models to further constrain the variations of the Earth's magnetic field for this time period, thus improving the archaeomagnetic dating technique.

ACKNOWLEDGEMENTS

This research was funded by the Spanish Ministry of Economy and Competitiveness, MINECO and the European Regional Development Fund (projects CGL2012-38481 and CGL2012-32149). AG acknowledges partial financial support given by PAPIIT IN-105214. We are grateful to E. Tema and an anonymous reviewer for their constructive reviews. We thank S. Torres and Bennacer Moussaid for their support in the field, as well as the archaeological team of Pinilla del Valle site.

REFERENCES

Borradaile, G. J., Lagroix, F., and Trimble, D., 2001, Improved isolation of archeomagnetic signals by combined low temperature and alternating field demagnetization, *Geophysical Journal International*, **147**, 176–82.

Calvo, M., Prévot, M., Perrin, M., and Riisager, J., 2002, Investigating the reasons for the failure of palaeointensity experiments: a study on historical lava flows from Mt, *Etna (Italy), Geophysical Journal International*, **149**(1), 44–63.

Carrancho, Á., Villalaín, J. J., Pavón-Carrasco, F. J., Osete, M. L., Straus, L. G., Vergès, J. M., Carretero, J. M., E., A.;. D., González Morales, M. R., Arsuaga, J. L., Bermúdez de Castro, J. M., and Carbonell, E., 2013, First directional European palaeosecular variation curve for the Neolithic based on archaeomagnetic data, *Earth and Planetary Science Letters*, **380**, 124–37.

Casas, L., and Incoronato, A., 2007, Distribution analysis of errors due to relocation of geomagnetic data using the Conversion via Pole (CVP) method: implications on archaeomagnetic data, *Geophysical Journal International*, **169** (2), 448–54.

Casas, L., Ramírez, J., Navarro, A., Fouzai, B., Estop, E., and Rosell, J. R., 2014, Archaeometric dating of two limekilns in an industrial heritage site in Calders (Catalonia, NE Spain), *Journal of Cultural Heritage*, **15**(5), 550–6.

Chauvin, A., Garcia, Y., Lanos, P., and Laubenheimer, F., 2000, Paleointensity of the geomagnetic field recovered on archaeomagnetic sites from France, *Physics of the Earth and Planetary Interiors*, **120**, 111–36.

Coe, R. S., 1967, Paleointensities of the Earth's magnetic field determined from Tertiary and Quaternary rocks, *Journal of Geophysical Research*, **72**, 3247–62.

Coe, R. S., Grommé, S., and Mankinen, E. A., 1978, Geomagnetic paleointensities from radiocarbon dated lava flows on Hawaii and the question of the Pacific nondipole low, *Journal of Geophysical Research, Solid Earth*, **83**, 1740–56.

Day, R., Fuller, M., and Schmidt, V. A., 1977, Hysteresis properties of titanomagnetites—grain size and compositional dependence, *Physics of the Earth and Planetary Interiors*, **13**, 260–7.

Donadini, F., Kovacheva, M., and Kostadinova, M., 2010, Archaeomagnetic study of ancient Roman lime kilns (1c. AD) and one pottery kiln (1c. BC – 1c. AD) at Krivina, Bulgaria, as a contribution to archeomagnetic dating, *Archeologia Bulgarica*, **XIV**(2), 213 – 25.

Dunlop, D. J., 2002, Theory and application of the Day plot (M_{rs}/M_s versus H_{cr}/H_c). 2. Application to data for rocks, sediments, and soils, *Journal of Geophysical Research*, **107**(B3), 1–15.

Dunlop, D. J., and Özdemir, Ö., 1997, *Rock magnetism: fundamentals and frontiers*, Cambridge University Press, New York.

Fisher, R., 1953, Dispersion on a sphere, *Proceedings of the Royal Society London A*, **217**, 295–305.

Gallet, Y., Genevey, A., and LeGoff, M., 2002, Three millennia of directional variation of the Earth's magnetic field in Western Europe as revealed by archaeological artefacts, *Physics of the Earth and Planetary Interiors*, **131**, 81–9.

García Menárguez, A., 2004, Sobre la producció de calç durant l'època romana en la comarca del Baix SeguraL la calera del Moncaio (Guardamar), *La Rella*, **17**, 23–38.

Genevey, A., and Gallet, Y., 2003, Eight thousand years of geomagnetic field intensity variations in the eastern Mediterranean, *Journal of Geophysical Research*, **108**(B5), 2228. DOI: 10.1029/2001JB001612.

Gómez-Paccard, M., Chauvin, A., Lanos, P., and Thiriot, J., 2008, New archeointensity data from Spain and the geomagnetic dipole moment in Western Europe over the past 2000 years, *Journal of Geophysical Research*, **113**, , B09103DOI: 10.1029/2008JB005582.

Gómez-Paccard, M., Chauvin, A., Lanos, P., McIntosh, G., Osete, M. L., Catanzariti, G., Ruiz-Martinez, V. C., and Núñez, J. I., 2006a, First archaeomagnetic secular variation curve for the Iberian Peninsula: comparison with other data from Western Europe and with global geomagnetic field models, *Geochemistry, Geophysics, Geosystems*, **7**, , Q12001DOI: 10.1029/2006GC001476.

Gómez-Paccard, M., Catanzariti, G., Ruiz-Martínez, V. C., McIntosh, G., Núñez, J. I., Osete, M. L., Lanos, P., Chauvin, A., Tarling, D. H., Bernal-Casasola, D., Thiriot, J., and Archaeological Working Group, 2006b, A catalogue of Spanish archaeomagnetic data, *Geophysical Journal International*, **166**, 1125–43.

Goguitchaichvili, A., Morales, J., Schavelzon, D., Vásquez, C., Gogorza, C., Loponte, D., and Rapalini, A., 2015, Variation of the Earth's magnetic field strength in South America during the last two millennia: new results from historical buildings of Buenos Aires and re-evaluation of regional data, *Physics of the Earth and Planetary Interiors*, **245**, 15–25.

Grommé, C. S., Wright, T. L., and Peck, D. L., 1969, Magnetic properties and oxidation of iron – titanium oxide minerals in Alae and Makaopuhi lava lakes, *Hawaii, Journal of Geophysical Research*, **74**, 5277 – 9.

Hagstrum, J. T., and Blinman, E., 2010, Archeomagnetic dating in western North America: an updated reference curve based on paleomagnetic and archeomagnetic data sets, Geochemistry, Geophysics, *Geosystems*, **11**(6) , Q06009, DOI: 10.1029/2009GC002979.

Hus, J., and Geeraerts, R., 1998, The direction of geomagnetic field in Belgium since Roman times and the reliability of archaeomagnetic dating, *Physics and Chemistry of the Earth*, **23**(9–10), 997–1007.

Jiménez de Gregorio, F., 1990, Apunte geográfico-económico de los pueblos de la actual provincia de Madrid en el 1752 (VII), *Anales del Instituto de Estudios Madrileños*, **XXVIII**, 243–72.

Kapper, K. L., Donadini, F., Mauvilly, M., Panovska, S., and Hirt, A. M., 2014, New directional archaeomagnetic data of burned cave sediments from Switzerland and geomagnetic field variations in Central Europe, *Geophysical Journal International*, **198**, 1208–21.

Karampaglidis, T., Benito-Calvo, A., and Pérez-González, A., 2015, Geomorphology of the Lozoya river drainage basin area (Community of Madrid, Spanish Central System), *Journal of Maps*, **11**(2), 342–53.

Kirschvink, J., 1980, The least-squares line and plane and the analysis of paleomagnetic data, *Geophysical Journal of the Royal Astronomical Society*, **62**, 699–718.

Korte, M., Donadini, F., and Constable, C. G., 2009, Geomagnetic field for 0–3 ka: 2. A new series of time-varying global models, *Geochemistry, Geophysics, Geosystems*, **10**(6) , Q06008, DOI: 10.1029/2008GC002297.

Kosterov, A. A., Perrin, M., Glen, J. M., and Coe, R. S., 1998, Paleointensity of the Earth's magnetic field in early Cretaceous time: the Parana Basalt, Brazil, *Journal of Geophysical Research*, **103**(B5), 9739–53.

Kovacheva, M., Boyadziev, Y., Kostadinova-Avramova, M., Jordanova, N., and Donadini, F., 2009, Updated archeomagnetic data set of the past 8 millennia from the Sofia laboratory, *Bulgaria, Geochemistry, Geophysics, Geosystems*, **10**, , Q05002DOI: 10.1029/2008GC002347.

Lanos, P. H., 2004, Bayesian inference of calibration curves: application to archaeomagnetism, in *Tools for constructing chronologies: crossing disciplinary boundaries (eds. C. Buck and A. Millard)*, 43–82, Springer, London.

Lengyel, S., 2010, The pre-AD 585 extension of the U.S. Southwest archaeomagnetic reference curve, *Journal of Archaeological Science*, **37**(12), 3081–90.

Leonhardt, R., 2006, Analyzing rock magnetic measurements: the RockMagAnalyzer 1.0 software, *Computers & Geosciences*, **32**, 1420–31.

Levi, S., 1977, The effect of magnetite particle size on paleointensity determinations of the geomagnetic field, *Physics of the Earth and Planetary Interiors*, **13**, 245–59.

Lowrie, W., 1990, Identification of ferromagnetic minerals in a rock by coercivity and unblocking temperature properties, *Geophysical Research Letters*, **17**, 159–62.

McClelland-Brown, E., 1984, Experiments on TRM intensity dependence on cooling rate, *Geophysical Research Letters*, **11**(3), 205–8.

Márquez, B., Mosquera, M., Pérez-González, A., Arsuaga, J. L., Baquedano, E., Panera, J., Espinosa, J. A., and Gómez, J., 2013, Evidence of a Neanderthal-made quartz-based technology at Navalmaíllo Rockshelter (Pinilla del Valle, Madrid region, Spain), *Journal of Anthropological Research*, **69**(3), 373–95.

Mazadiego Martínez, L. F., Puche, O., and Jordá, L., 2005, Caleras del Alto Valle del Lozoya: Rascafría y Pinilla del Valle, in *2° Simposio sobre la Minería y metalurgía históricas en el sudoeste europeo, 23–27 Junio 2004, Madrid*, 551–64, Sociedad Española para la Defensa del Patrimonio Geológico y Minero, Madrid.

Morales, J., Goguitchaichvili, A., Acosta, G., González, T., Alva-Valdivia, L., Robles-Camacho, J., and Hernández-Bernal, S., 2009, Magnetic properties and archeointensity determination on pre-Columbian pottery from Chiapas, *Mesoamerica, Earth Plantes Space Special Issue*, **61**, 83–91.

Morales, J., Goguitchaichvili, A., Aguilar-Reyes, B., Pineda-Duran, M., Camps, P., Carvallo, C., and Calvo-Rathert, M., 2011, Are ceramics and bricks reliable absolute geomagnetic intensity carriers? *Physics of the Earth and Planetary Interiors*, **187**, 310–21.

Ordinas i Marcé, G., 1995, *Els forns de calç a Santa Maria del Camí, Edicions de l'Ajuntament*, Santa Maria del Camí.

Pavón-Carrasco, F. J., Osete, M. L., Torta, J. M., and Gaya-Piqué, L. R., 2009, A regional archeomagnetic model for Europe for the last 3000 years, SCHA.DIF.3 K: applications to archeomagnetic dating, *Geochemistry, Geophysics, Geosystems*, **10**, , Q03013DOI: 10.1029/2008GC002244.

Pavón-Carrasco, F. J., Rodríguez-González, J., Osete, M. L., and Torta, J. M., 2011, A MATLAB tool for archaeomagnetic dating, *Journal of Archaeological Science*, **38**, 408–19.

Porrúa Martínez, A., 2006, Los hornos de cal de la villa romana de El Salero (S. Pedro del Pinatar): un ejemplo de la interacción entre instalaciones industriales rurales y la reutilización de materiales constructivos, *AnMurcia*, **22**, 117–47.

Prevosti, M., Casas, L., Roig Pérez, J. F., Fouzai, B., Álvarez, A., and Pitarch, A., 2013, Archaeological and archaeomagnetic dating at a site from the ager Tarraconensis (Tarragona, Spain): El Vila-sec Roman pottery, *Journal of Archaeological Science*, **40**(6), 2686–701.

Reimer, P. J., Bard, E., Bayliss, A., Beck, J. W., Blackwell, P. G., Bronk Ramsey, C., Buck, C. E., Cheng, H., Edwards, R. L., Friedrich, M., Grootes, P. M., Guilderson, T. P., Haflidason, H., Hajdas, I., Hatté, C., Heaton, T. J., Hogg, A. G., Hughen, K. A., Kaiser, K. F., Kromer, B., Manning, S. W., Niu, M., Reimer, R. W., Richards, D. A., Scott, E. M., Southon, J. R., Turney, C. S. M., and van der Plicht, J., 2013, IntCal13 and Marine13 radiocarbon age calibration curves 0–50,000 years cal BP, *Radiocarbon*, **55**(4), 1869–87.

Schnepp, E., and Lanos, P., 2005, Archaeomagnetic secular variation in Germany during the past 2500 years, *Geophysical Journal International*, **163**, 479–90.

Senegacnik, A., Oman, J., and Sirok, B., 2007, Analysis of calcination parameters and the temperature profile in an annular shaft kiln. Part 2: results of tests, *Applied Thermal Engineering*, **27**, 1473–82.

Stacey, F. D., 1967, The Koenigsberger ratio and the nature of thermoremanence in igneous rocks, *Earth and Planetary Science Letters*, **2**, 67–8.

Stillinger, M. D., Feinberg, J. M., and Frahm, E., 2015, Refining the archaeomagnetic dating curve for the Near East: new intensity data from Bronze Age ceramics at Tell Mozan, *Syria, Journal of Archaeological Science*, **53**, 345–55.

Tauxe, L., Butler, R., Banerjee, S., and van der Voo, R., 2010, *Essentials of paleomagnetism*, University of California Press, San Diego, CA.

Tema, E., and Lanza, R., 2008, Archaeomagnetic study of a lime kiln at Bazzano (northern Italy), *Physics and Chemistry of the Earth*, **33**(6–7), 534–43.

Tema, E., and Kondopoulou, D., 2011, Secular variation of the Earth's magnetic field in the Balkan region during the last eight millennia based on archaeomagnetic data, *Geophysical Journal International*, **186**, 603–14.

Tema, E., Hedley, I., and Lanos, P., 2006, Archaeomagnetism in Italy: a compilation of data including new results and a preliminary Italian secular variation curve, *Geophysical Journal International*, **167**, 1160–71.

Tema, E., Fantino, C., Ferrara, E., Lo Giudice, A., Morales, J., Goguitchaichvili, A., Camps, P., Barello, F., and Gulmini, M., 2013, Combined archaeomagnetic and thermoluminescence study of a brick kiln excavated at Fontanetto Po (Vercelli, northern Italy), *Journal of Archaeological Science*, **40**, 2025–35.

Thellier, E., and Thellier, O., 1959, Sur l'intensité du champ magnétique terrestre dans le passé historique et géologique, *Annales de Géophysique*, **15**, 285–376.

Ventolà, L., Vendrell-Saz, M., and Giraldez, P., 2012, Consolidation of stone blocks prior to placement: a case study of the Roman wall in Tarragona (Spain): report and methodology, *Journal of Cultural Heritage*, **13**, 437–41.

Zananiri, I., Batt, C. M., Lanos, P., Tarling, D. H., and Linford, P., 2007, Archaeomagnetic secular variation in the UK during the past 4000 years and its application to archaeomagnetic dating, *Physics of the Earth and Planetary Interiors*, **160**(2), 97–107.